2-1-2020

Mud deposition and diagenesis within an Early Palaeozoic clinothem: Power Steps Formation, Newfoundland, Canada

Kathryn C. Denommee
Exxon Mobil Corporation

Dario Harazim
University of Calgary

Samuel J. Bentley
Louisiana State University

James H. MacQuaker
Exxon Mobil Corporation

Stefanie Lode
Memorial University of Newfoundland

See next page for additional authors

Recommended Citation

Denommee, K., Harazim, D., Bentley, S., MacQuaker, J., Lode, S., & Olanipekun, B. (2020). Mud deposition and diagenesis within an Early Palaeozoic clinothem: Power Steps Formation, Newfoundland, Canada. *Geological Magazine, 157* (2), 134-148. https://doi.org/10.1017/S0016756819000402

Geological Magazine

www.cambridge.org/geo

Mud deposition and diagenesis within an Early Palaeozoic clinothem: Power Steps Formation, Newfoundland, Canada

Kathryn C. Denommee[1,*], Dario Harazim[2,3], Samuel J. Bentley[3], James H. Macquaker[1], Stefanie Lode[4] and Babatunde John Olanipekun[4]

[1]ExxonMobil Upstream Research Company, 22777 Springwoods Village Parkway, Spring, TX 77389, USA; [2]Department of Geosciences, University of Calgary, 2500 University Drive NW, Calgary, Alberta, T2N 3X5, Canada; [3]Department of Geology and Geophysics, Howe-Russel-Kniffen Geoscience Complex, Louisiana State University, Baton Rouge, LA 70803, USA and [4]Department of Earth Sciences, Memorial University of Newfoundland, 300 Prince Philip Drive, St John's, Newfoundland, A1B 3X5, Canada

Original Article

Cite this article: Denommee KC, Harazim D, Bentley SJ, Macquaker JH, Lode S, and Olanipekun BJ (2020) Mud deposition and diagenesis within an Early Palaeozoic clinothem: Power Steps Formation, Newfoundland, Canada. *Geological Magazine* **157**: 134–148. https://doi.org/10.1017/S0016756819000402

Received: 20 September 2018
Revised: 16 March 2019
Accepted: 2 April 2019
First published online: 28 May 2019

Author for correspondence: Kathryn C. Denommee,
Email: kathryn.c.denommee@gmail.com

Abstract

The early Ordovician (~385 Ma) Power Steps Formation, Newfoundland, Canada, exposes a well-preserved mudstone-dominated clinothem that serves as an excellent archive for understanding how mud has been produced, transported and converted into mudstone prior to the evolution of globally widespread, deep soil horizons. Sedimentological analysis of four sandstone and five mudstone facies, along the Ochre Cove clinothem, reveal that mud and sand were delivered by unidirectional currents and experienced episodic reworking by storm waves. Petrographic examination and X-ray diffraction from described mudstone facies reveal significant variability in the distribution of illite versus chlorite between the lower and upper part of the Ochre Cove clinothem. This research highlights that in the present-day clay mineral fraction, illite is often detrital whereas chlorite originated via the alteration of silt-sized, highly unstable, mafic (volcanoclastic?) grains. Throughout all sedimentologic facies, albeit in different proportions, these mafic lithic grains were diagenetically altered via *in situ* weathering before significant compaction occurred, resulting in the precipitation of significant volumes of pore-bridging, silica- and iron-rich chlorite cement. Compositional, diagenetic and textural attributes across the Ochre Cove mud clinothem vary as a function of starting composition, hydrodynamic sorting and grain density. Given that a significant proportion of clay minerals has been generated via *in situ* transformation of a mafic, non-stable precursor assemblage, we recommend future studies to incorporate detailed petrographic description along with X-ray diffraction analyses when aiming to employ trends in whole-rock clay mineral data as a proxy in provenance and palaeoclimate studies of very old (pre-Devonian) mudstones and sandstones.

1. Introduction

Well-preserved, fine-grained deltaic systems reveal links between oceanographic conditions, input, dispersal and biologic mixing of a wide range of grain sizes that together control the distribution of sedimentary facies on the continental shelf (e.g. Aigner & Reineck, 1982; Potter *et al.* 2005; Clifton, 2007; Milligan *et al.* 2007; Plint *et al.* 2012; Hart *et al.* 2013; Plint, 2014; Poyatos-Moré *et al.* 2016; Schieber, 2016; Laycock *et al.* 2017; Li & Schieber, 2018). Relative to our understanding of sand-rich sedimentary facies, the products of muddy sediment transport and deposition are less well understood, even in modern settings (Wright *et al.* 2001; Cattaneo *et al.* 2003, 2007; Jaramillo *et al.* 2009; Hanebuth *et al.* 2015; Denommee *et al.* 2016; Eidam *et al.* 2017; Shchepetkina *et al.* 2017; Shanmugam, 2018). The reason for this knowledge gap is that primary mud depositional fabrics, such as lamina- and bedding-, are (a) difficult to observe with the naked eye (e.g. Schieber, 1999; Potter *et al.* 2005) and (b) frequently overprinted by post-depositional processes including bioturbation and compaction (e.g. Egenhoff & Fishman, 2013), as well as by other diagenetic processes including dissolution, alteration and replacement (Hower *et al.* 1976; Bjørlykke, 1998; Bentley *et al.* 2006; Bhattacharya & MacEachern, 2009; Buatois *et al.*, 2011; Harazim *et al.* 2015; Harazim & McIlroy, 2015).

This contribution reaches beyond the approaches developed for describing sandstone and systematically investigates the compositional, diagenetic and textural alterations of early Palaeozoic mudstone as a function of hydrodynamic sorting and reworking along an onshore–offshore dispersal path. The Cambrian–Ordovician succession on Bell Island (Fig. 1) preserves >1 km-thick siliciclastic sandstone and mudstone that were deposited by wave-, current- and gravity-driven processes in a shallow marine setting (Ranger *et al.* 1984; Brenchley *et al.* 1993; Harazim & McIlroy, 2015). Since studies focused on the sedimentary evolution of early Palaeozoic mud clinothems are extremely rare, the Power Steps Formation

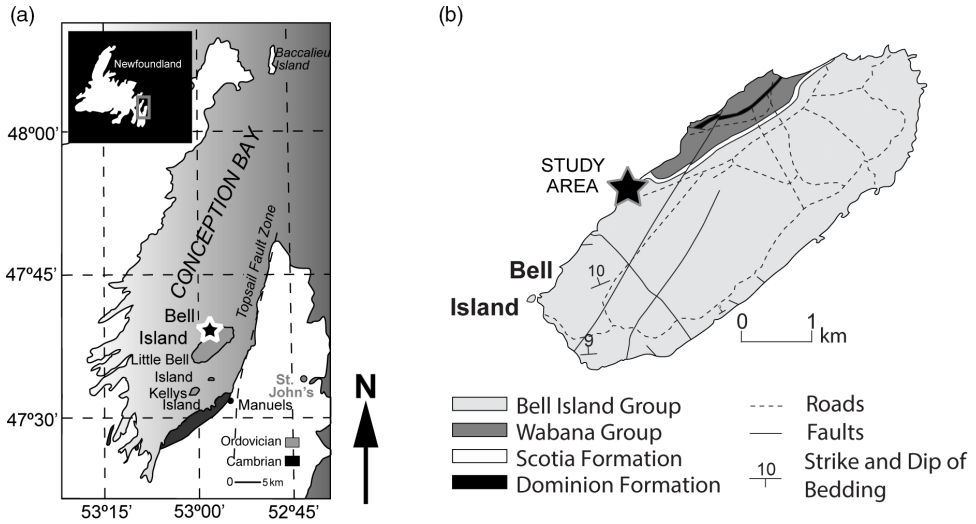

Fig. 1. (a) Topographic map of Eastern Newfoundland, indicating the location of Bell Island inside Conception Bay. (b) Simplified geological map of Bell Island, Newfoundland, with the location of the study area at Ochre Cove (black star).

serves as a new key archive for understanding early Palaeozoic shelf-building processes where most of the detrital components have been delivered via mechanical weathering from a non-vegetated hinterland. As part of the Power Steps Formation, the fully exposed muddy Ochre Cove clinothem (OCC, Figs 1, 2) offers a unique opportunity to investigate (1) the nature and varying mechanisms of sediment dispersal across an early Ordovician clinothem and (2) how post-depositional changes, in particular burial diagenesis, govern the distribution of chlorite and illite cement across the OCC.

2. Study area and geological overview

The study area is located in the Avalon Zone, the easternmost tectonostratigraphic zone of the Newfoundland Appalachians (Williams, 1979; Van Staal *et al.* 2012), and consists of three major assemblages of predominantly late Precambrian to Lower Cambrian volcanic, volcaniclastic and sedimentary rocks. In the eastern part of the Conception Bay area, the Lower Ordovician (Arenigian ~478–472 Ma) interval is preserved and exposed at Ochre Cove on Bell Island. This interval records the transition between the Bell Island and Wabana Groups (Figs 1, 2). During early Ordovician times, the Avalon Zone is suggested to be located on the western margin of Gondwana (Cocks & Torsvik, 2002; Van Staal *et al.* 2012). Rapid subsidence and contemporaneous sea-level rise (Austermann, 2016) provided the accommodation necessary to deposit the deep- to shallow-marine Bell Island and Wabana Group strata, which are presumed to unconformably overlie Precambrian Gondwanan continental crustal rocks (Miller, 1983; Ranger *et al.* 1984).

The muddy OCC is located on N-NW Bell Island ('Locality I' of Ranger *et al.* 1984) and is preserved along 60 m tall cliffs, which fully expose dipping clinoform surfaces that were identified in this study as foreset, topsets and possible bottomsets (Fig. 3). At the base of the exposure, the uppermost Bell Island Group exposes oolitic, chamositic ironstone, onto which the Wabana Group strata downlap (Ranger *et al.* 1984) (Figs 2, 3). As a whole, the lowermost Power Steps Formation is composed of interbedded, clay-rich, silt-bearing mudstones and subordinate, decimetre-thick sandstones (Fig. 3). The lowermost part of the Power Steps Formation (Youngster's Gulch Member) is composed of clay- and silt-rich mudstone that is interbedded with centimetre- to decimetre-thick medium- to coarse-grained sulfide-rich sandstone (Ranger *et al.* 1984) (Fig. 3). The formation has previously been interpreted as being deposited in a tidally dominated deltaic environment (Ranger *et al.* 1984), with detrital components sourced from the Precambrian Harbour Main, Conception and Cabot groups, as well as from the Holyrood plutonic series (e.g. Bruckner, 1969).

3. Materials and methods

3.a. Characterization of sedimentary fabric and texture

In order to examine the sedimentary processes responsible for the deposition of the OCC, the succession was logged at centimetre scale from continuous section (Fig. 2). Large (up to 50 cm in diameter), oriented hand samples ($n = 35$) of unweathered mudstone and sandstone were collected from the cliff face, stabilized with epoxy resin and slabbed in the laboratory. Petrographic thin-sections (thickness ~25 μm) were prepared from select slabbed intervals and scanned at high resolution using a flatbed film scanner. Descriptions of texture, fabric, bedding contacts and bioturbation indices (*sensu* Taylor & Goldring, 1993) from outcrop, hand specimen and petrographic thin-sections were integrated in order to generate facies descriptions that also reveal the most likely origin of framework components (grain versus cement). Mudstones were described using the methodologies of Campbell (1967) and Lazar *et al.* (2015), in order to constrain both depositional environment and sediment transport mechanisms. Nine genetically related sandstone and mudstone facies have been grouped based on their palaeoenvironmental context into two facies associations (FAs).

3.b. Compositional analysis

Quantitative X-ray diffraction (QXRD) has been performed on 13 powder samples, which cover all sedimentologic facies. The pronounced stratigraphic trends for the most common minerals illite, chlorite and quartz have been captured. For QXRD analyses, ~2 g of crushed material was processed in ethanol and micronized in a McCrone mill for ~3 min. Samples were then dried at 60 °C and disaggregated using a mortar and pestle. Randomly oriented sample material was loaded into aluminium sample holders following

https://doi.org/10.1017/S0016756819000402

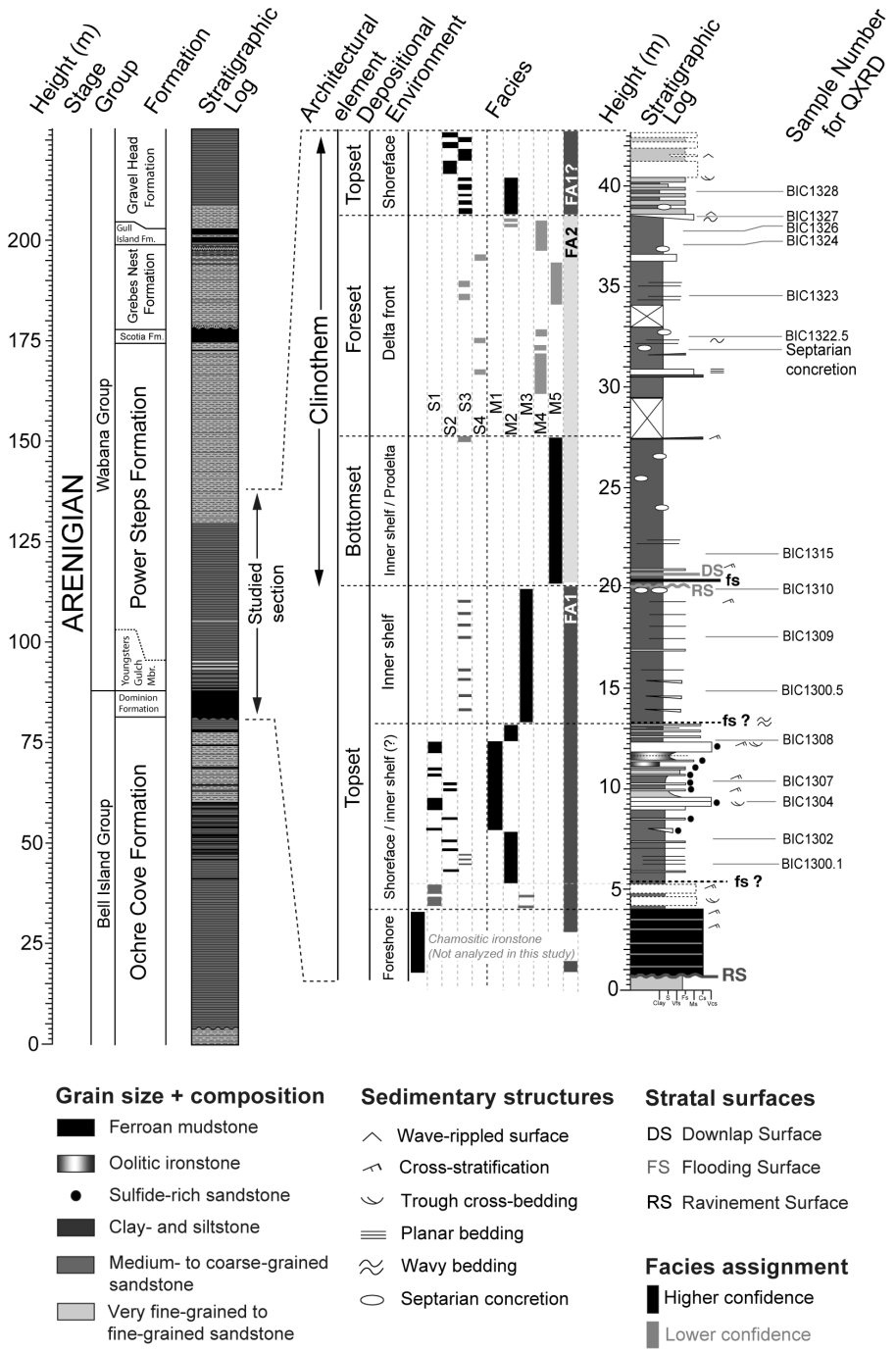

Fig. 2. Generalized stratigraphic log of the OCC exposure at Ochre Cove, Bell Island, Newfoundland, indicating the stratigraphic position of facies, sampling locations for QXRD analyses and interpreted depositional environments.

the methods of Poppe *et al.* (2001). For clay mineral analysis, the size fraction equivalent to <2 μm spherical diameter of quartz was separated by dispersing a representative sample of whole rock powder in a 0.1 % sodium phosphate solution and extracting particles from the upper 5 cm of suspension after settling for 3 hours 10 minutes as determined by Stokes' law. Oriented clay smears were prepared following the methods of Moore & Reynolds (1997).

X-ray diffraction (XRD) data were collected using a Panalytical Empyrean X-ray diffractometer with Cu Kα radiation (40 kV and 20 mA). For clay mineral analysis, XRD runs were performed for each sample after each of the following four steps: (1) air-drying; (2) ethylene glycol salvation at 25 °C for a minimum of 8 hours; (3) heating at 300 °C for 1 hour; and (4) heating at 550 °C for 1 hour. Clay minerals were identified by comparing peak positions and intensity of basal (001) reflections on the four XRD diagrams (Moore & Reynolds, 1997; Poppe *et al.* 2001). Semi-quantitative determination of bulk and clay mineral composition was facilitated by using MacDiff software (Petschick, 2001), with the uncertainty in XRD analysis estimated at ±5 %. For clay, mineral abundances are based on peak areas and normalized to Smectite + Illite + Kaolinite + Chlorite = 100 %. Grain boundaries and intergranular pore space filling have been visually examined.

https://doi.org/10.1017/S0016756819000402

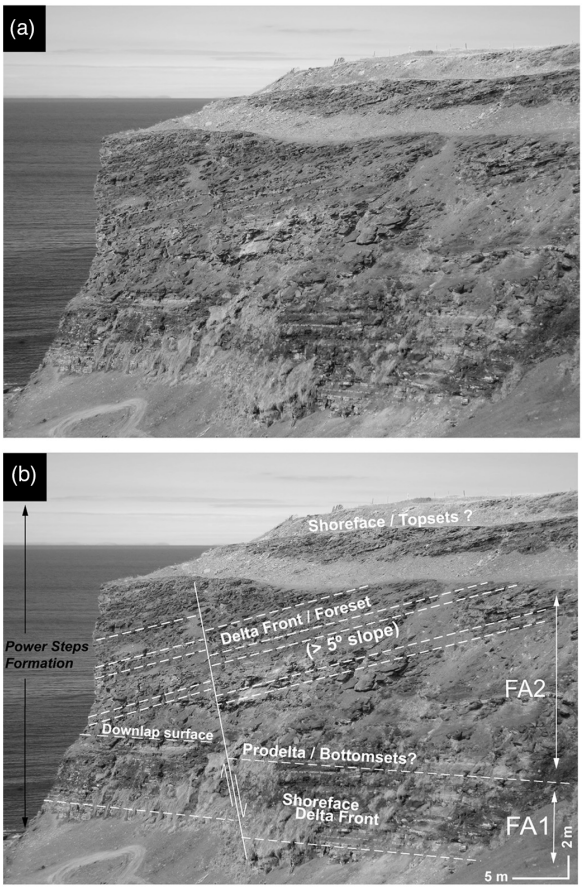

Fig. 3. (a) Field view of the clinothem exposure (Youngster's Gulch Member and Power Steps Formation) at Ochre Cove, Bell Island, Newfoundland. (b) Annotated view of the clinothem exposure indicating the architectural elements and major facies associations.

3.c. Scanning electron microscopy (SEM)

Composition and sedimentary fabrics of representative samples from each facies were undertaken from polished thin sections using a JEOL JSM-7600F Thermal Field Emission Scanning Electron Microscope (SEM) equipped with an Oxford Instruments Aztec Energy Dispersive X-ray System and a silicon drift detector. Images were obtained primarily in backscattered mode utilizing a JEOL solid-state backscatter detector. Imaging conditions were 15 kV and 8 mm working distance. Polished thin-sections were prepared for SEM imaging by lightly cleaning the thin-section surface with methanol using low-lint cloths, air-dried and then coated with *c.* 30 nm of carbon using a Cressington 208 carbon evaporator. Particular attention was paid to the amount and type of grain dissolution, cementation as well as replacement, as an indicator for *in situ* weathering and generation of clay minerals, chlorite, and quartz cement (Figs 4–8; see discussion).

4. Facies and facies associations

4.a. Facies descriptions

Nine sedimentary facies, four sandstone facies and five mudstone facies were recognized in this study. Sedimentary facies were identified by integrating hand specimen observations, thin-section petrography, and QXRD analyses. Sandstone and mudstone facies are described separately. The stratigraphic distribution of bioturbation style and intensity as well as the main mineral trends in the mudstones follow the description of individual facies.

4.b. Facies S1: amalgamated sandstone

4.b.1 Description

Facies S1 comprises less than 10 % of the studied section. This facies is characterized by fine- to medium-grained, continuous sandstone units, with internally discontinuous, often amalgamated erosive-based, centimetre- to decimetre-thick, thin-bedded, beds and bedsets (Fig. 4a). These internal beds and bedsets contain steep (>10°) bidirectional ripples with broad scours that are overlain by long-wavelength wave ripples with upward-flattening lamina sets (Fig. 4b). S1 sandstones are sparsely bioturbated (BI 1–2, 5–30 % *sensu* Taylor & Goldring, 1993). The most common trace fossils observed include compacted *Planolites* (Fig. 4c). The S1 framework is composed of predominantly detrital, well-cemented quartz embedded within a sand-sized pseudomatrix of diagenetically altered lithic fragments. Minor components include detrital biotite and muscovite, with remnants of plagioclase and heavy accessory minerals (Fig. 4d).

4.b.2. Interpretation

Relatively continuous S1 sandstone beds (>10 m continuity) (Fig. 4a) with a vertical division of erosive-based wave ripples with increasing wavelength are interpreted as having been deposited by possibly combined flows with relatively long wavelengths (Clifton, 2007). Well-preserved bidirectional wave ripples with long wavelengths are indicative of sediment reworking and lateral transport under the influence of wave action; wave-ripple erosion might also indicate a (weak) unidirectional component operating during deposition (Duke *et al.* 1991; Myrow & Southard, 1996) (Fig. 6b, further below).

The absence of significant volumes of detritally derived, clay-rich material within S1 sandstone may imply deposition under initially very low clay concentration (little to no interstratified mud) or an initially fast aggradation of sand-sized material. The presence of wave-reworked tops and significant breaks in sedimentation without change in grain size argues for occasional erosion and possibly redeposition (Fig. 4b). A thin top layer with mainly fine-grained sandstone-filled *Planolites* within this coarser-grained S1 sandstone and some other biodeformational structures indicates potential bypass of the finer grain-size fraction downstream (Fig. 4b).

4.c. Facies S2: lenticular sandstone

4.c.1. Description

Lenticular sandstone makes up less than 5 % of the studied section. This facies appears as centimetre-thick, erosive-based, laterally discontinuous, very fine-grained sandstones that are interbedded with wave-reworked mudstone of facies M2 (Fig. 5a–d). S2 sandstone contains current or possible combined-flow ripples (Fig. 5b). S2 sandstones appear generally non-bioturbated. Framework grains include predominantly detrital quartz, diagenetic chlorite cement, lithic clasts and detrital biotite together with some muscovite.

4.c.2. Interpretation

The highly variable distribution of this facies indicates that supply of sand has not been continuous throughout the deposition of this facies. Internally curved, non-even lamination (Fig. 5b) indicates that ripples have not been deposited entirely via current-dominated processes, but transport also might have included an oscillatory component. Lamina geometries resembling wave-reworking

https://doi.org/10.1017/S0016756819000402

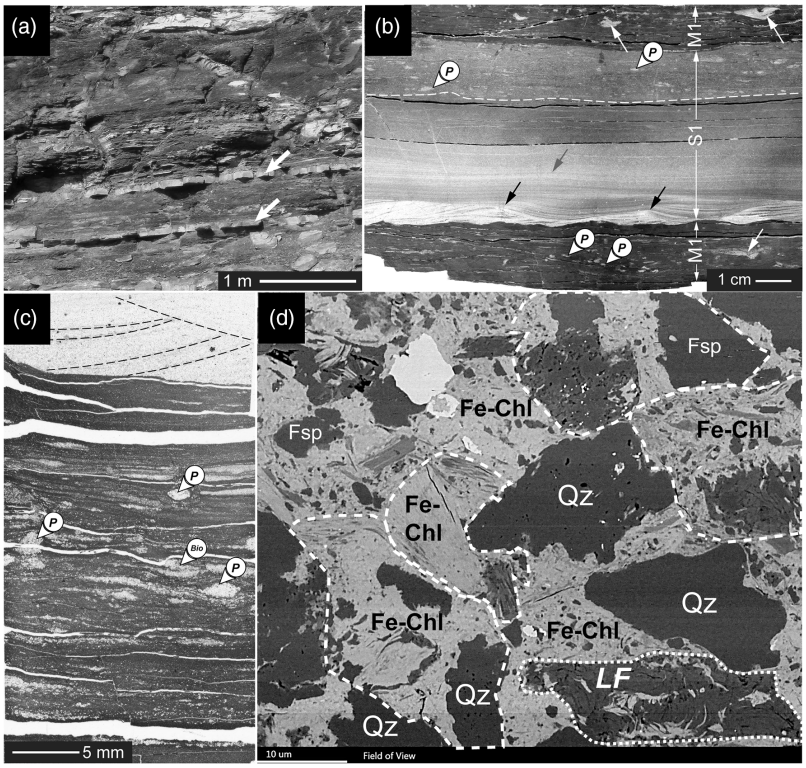

Fig. 4. Facies S1 and M1. (a) Outcrop photograph showing decimetre-thick S1 sandstone beds interbedding with decimetre- to metre-thick M1 mudstone. (b) Polished hand sample of fine- to medium-grained sandstone consisting of asymmetric (possibly combined-flow) ripples (black arrows) overlain by possibly combined-flow ripples with long wave periods (grey arrow). S1 sandstones internally exhibit erosional contacts (white dashed line). The interbedded M1 mudstone contains sandstone-filled gutters (white arrows) and sparse, millimetre-sized sand-filled *Planolites* burrows (P). (c) Close-up micrograph of M1 mudstone (perpendicular to bedding, flat bed scan). M1 mudstones are faintly laminated with elongated silty streaks and burrow fills of medium-grained chloritized grains and lithoclasts. (d) Low-resolution micrograph of M1 with dominant replacement mineralogy (plane-polarized light, perpendicular to bedding). Note how Fe-enriched chlorite with well-developed replacement fabric (white, dashed polygons, Fe–Chl) and in authigenically replaced lithic fragments (LF) dominate a large portion of the M1 mudstone. 'Floating' quartz grains (Qz) and remnants of Felspar (Fsp) are also present.

could point to the fact that these sandstone patches were differentially compacted starved ripples, similar to the ones described by Schieber *et al.* (2010). While during an initial erosion event (i.e. storm) a previous sand bed was reworked and mostly removed, the ripple trails indicate the lateral transport during the waning phase of the storm, which also entails preferential preservation within gutters and other local topographic depressions distributed over the seabed. If this scenario is correct, then the thin, disconnected sandstone lenses and laminae represent ripple tails (Schieber *et al.* 2010).

4.d. Facies S3: storm-reworked sandstone

4.d.1. Description

Facies S3 makes up *c.* 20 % of the overall exposure at Ochre Cove. The S3 sandstones comprise thin-bedded (5–10 cm thick), fine-grained sandstone with laterally (at metre-scale) continuous units that exhibit wavy and even contacts (Fig. 6a, b). Internally, S3 sandstones exhibit laterally continuous sets of centimetre-sized dunes with partially eroded tops (Fig. 6a) Single dunes include well-developed sets of dark-coloured laminae (Fig. 6a) and, occasionally, millimetre-thick backflow ripples (Fig. 6b). Framework components comprise quartz within a pseudomatrix of chloritized lithic fragments. Minor components include biotite, muscovite and plagioclase. Some framboidal pyrite is present as well. S3 sandstones are non-bioturbated to sparsely bioturbated (BI 0–1, 0–5 %) and contain rare, vertical, decimetre-long, possible escape traces (*Esc*, Fig. 6a).

4.d.2. Interpretation

The unidirectional ripple sets with backflow ripples possibly represent reactivation surfaces formed during current reversal. Given that S3 sandstones are preferentially located in near-shore facies (delta top in Figs 2, 3), a combination between fluvial and tidal influence is plausible. Frequently eroded tidal dune beds are sharply overlain by M3 mudstones (Fig. 6a). The tidal influence inferred for S3 sandstones is supported by the fact that the entire unit is non-bioturbated. Permanently changing salinities with episodically brackish conditions could have put additional stress on any infauna and therefore prevented colonization. Another possibility is that bioturbated tops were eroded during storm events.

4.e. Facies S4: planar-laminated sandstone

4.e.1. Description

This facies covers *c.* 5 % of the entire succession (Fig. 2). S4 sandstones appear as decimetre-thick, erosive-based, laterally highly continuous beds with non-even contacts (Fig. 7a). Individual units contain planar-bedded, normally graded fine- to medium-grained sandstone with muddy tops that belong to mudstone facies M4 (Fig. 7b, c). The tops of individual, erosive-based S4 event beds contain elongated, well-cemented septarian horizons and septarian concretions composed of brownish/reddish (possibly) ferroan carbonate (Fig. 7b). In hand specimen, S4 facies appear non-bioturbated. The framework is composed of angular quartz, lithic clasts, biotite and some minor plagioclase and muscovite.

https://doi.org/10.1017/S0016756819000402

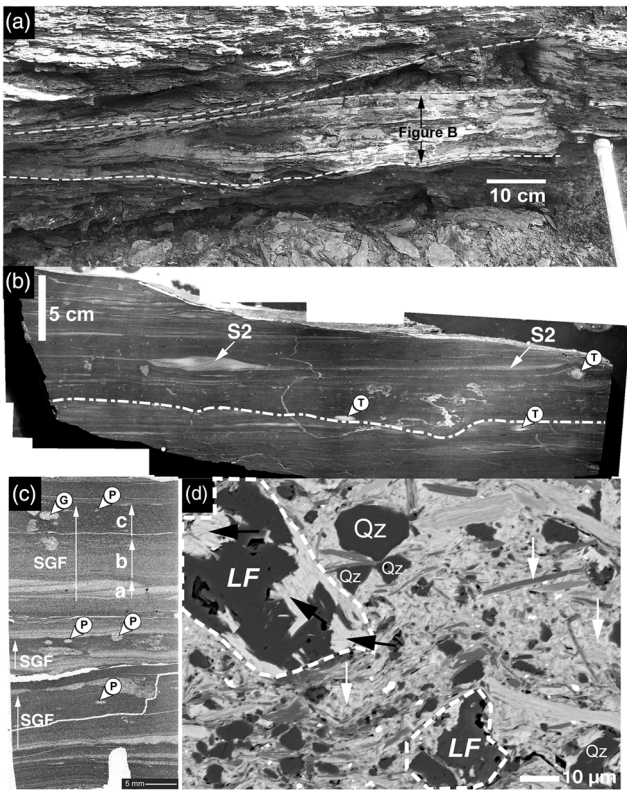

Fig. 5. Facies S2 and M2. (a) Outcrop view of mud-dominated facies M2, showing curved bed contacts and possible mud-on-mud erosional contacts (white dashed lines). (b) Polished hand sample of M2 mudstone, showing starved, asymmetric wave (possibly combined-flow) ripples (white arrows) of facies S2. Continuous, centimetre-wide erosional mud-on-mud contacts (white dashed line) are common in this facies. (c) Close-up micrograph showing centimetre-thick event beds (sediment gravity flows, SGFs) with a cross-laminated base (unit a), overlain by a laminated silty middle portion (unit b) and a bioturbated silt-rich mudstone (unit c). Clay-rich tops contain occasionally *Gyrolithes* (G), *Planolites* (P) and *Trichophycus* (T). (d) High-power SEM micrograph (backscatter mode) shows silt-sized, authigenically replaced mafic lithoclasts (LF, black arrow), engulfed within a 'pseudo-matrix' of Fe-rich chlorite cement (white arrow) that also include 'floating' quartz (Qz) grains.

4.e.2. Interpretation

The presence of erosive-based, laterally highly continuous, graded event beds with little evidence for post-depositional reworking indicates deposition from a depletive flow, such as a turbidity current (e.g. Talling *et al.* 2012). The vertical bed thickness of several decimetres and its stacked nature in conjunction with laterally continuous beds that can be traced across the entire OCC exposure (Fig. 7a) indicate deposition from depletive currents across large parts of the clinothem.

4.f. Facies M1: thick, continuous mudstone

4.f.1. Description

This facies was only observed in the lower part of the OCC and makes up less than 10 % of the overall succession (Fig. 2). M1 mudstone facies are developed as decimetre-thick, continuous mudstone beds with wavy bed contacts that also encase subordinate, centimetre-wide, sandstone-filled gutters (Fig. 4a, b). The bioturbation intensity is sparse to moderate (BI 1–2; 5–30 %) and consists of predominantly compacted, sandstone-filled, centimetre-sized *Planolites* burrows (Fig. 4c). Bed tops are moderately bioturbated by millimetre-sized *Planolites* and biodeformational structures (Fig. 4c). The framework of facies M1 contains very fine-grained to coarse silt-sized angular and subrounded quartz floating in a matrix of silt-sized, partially chloritized lithic fragments and mafic minerals, together with chlorite and illite that make up the matrix of this mudstone (Fig. 4d). Minor M1 components encompass biotite, muscovite and very little plagioclase (Fig. 4d).

4.f.2. Interpretation

Decimetre-thick, continuous mudstone beds intially encompassed a wide grain-size distribution that initially contained a large volume of silt, very fine-grained sized, potentially highly weathering susceptible minerals and (volcanoclastic) rock fragments (Fig. 4d). This mineral assemblage indicates deposition under rapidly decelerating flows, possibly from submarine flows with an initially high volcaniclastic content (pyroclastic currents?). Coarse-grained mud with high volumes of weathering-susceptible grains could also have been delivered from suspension settling of dense volcaniclastic clouds, after volcanic eruptions in the hinterland or after settling from plumes that eroded ash from a non-vegetated hinterland (Harazim & McIlroy, 2015). At this point it cannot be determined if the absence of grading within M1 mudstones reflects primary sedimentation, or if this represents a weathering artefact.

4.g. Facies M2: wave-reworked mudstone

4.g.1. Description

Facies M2 makes up the central part of the exposed OCC (less than 10 % of the entire exposure) (Fig. 5). Decimetre-thick M2 mudstone beds are highly discontinuous with even and wavy contacts and exhibit, internally, either one or two grain-size breaks (Fig. 5a, b). At bed scale, M2 mudstone contains subparallel, discontinuous, normally-graded medium silt- and clay-rich laminae that often preserve a prominent triplet motif (Fig. 5c, motif A–C). Mud-on-mud erosion is common in this facies. M2 mudstones are non- to sparsely bioturbated (BI 0–2; 0–30 %) comprising sandstone-filled *Planolites* and rare *Gyrolites*, preferentially confined to bed tops (Fig. 5c). Internally, M2 mudstone is composed of subangular to rounded, fine to medium silt-sized quartz, lithic clasts, biotite, some plagioclase and muscovite. The M2 matrix is predominantly composed of chlorite which shows intense replacement fabric within and around lithoclasts (Fig. 5d).

4.g.2. Interpretation

In M2 mudstones, well-preserved, highly continuous, erosion surfaces cross-cut partially preserved centimetre-thick clay- and siltstone-rich mudstone beds. This type of partial mudstone bed preservation is commonly the product of slow accumulation and periodic storm-wave reworking (Harazim & McIlroy, 2015). The preservation of centimetre-sized, partly erosive starved ripples with asymmetric lamination (facies S4) indicates that mud delivery to the seafloor is pulsed, alternating with periods of lateral sand transport but without significant aggradation (Schieber & Yawar, 2009). The intercalated, thin (millimetre-thick) beds with highly discontinuous lamina sets indicate periods of mud deposition that were most likely dominated by oscillating or even combined flows, possibly above the fair-weather wave base (Denommee *et al.* 2016) (Fig. 5c).

https://doi.org/10.1017/S0016756819000402

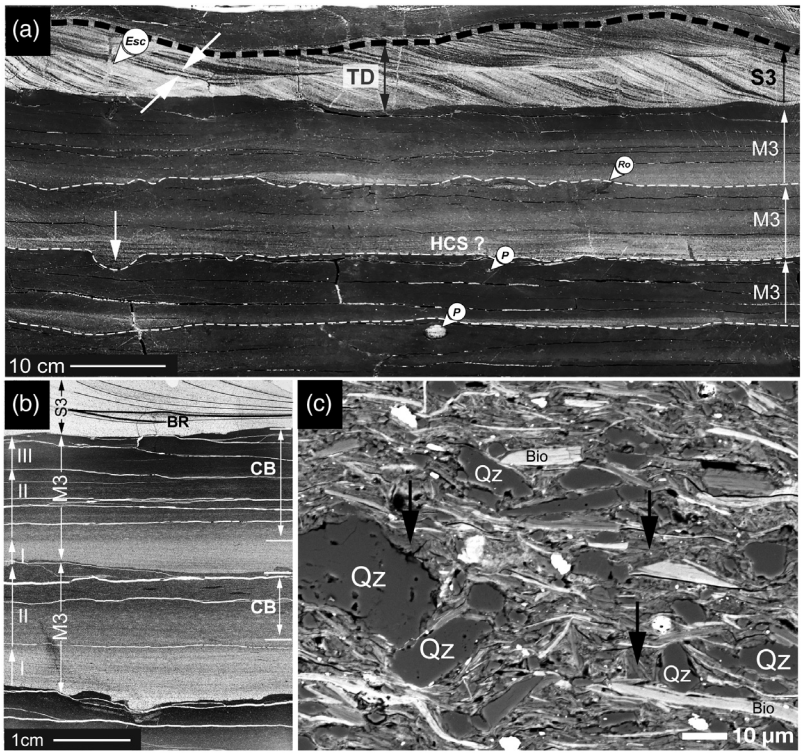

Fig. 6. Facies S3 and M3. (a) Close-up photograph of a large, polished hand sample resolving S3 sandstones and interbedded M3 mudstone. Medium-grained sandstone-filled gutters (white arrow) are overlain by pinch-and-swell lamination (small hummocky cross-stratified (HCS) beds?). Clay-rich bed tops contain a palimpsest ichnofaunal assemblage composed of *Planolites* (P) and *Rosselia* (Ro). Laterally continuous centimetre-thick, partially eroded, potential three-dimensional tidally influenced dune-scale bedforms (TD, grey arrows) comprise facies S3. Those tidal dunes have eroded tops (black dashed line) and include prominent tidal bundling (white, opposing arrows). (b) Cross-section through facies M3 mudstone showing the tripartite subdivision of partially eroded, stacked, potential HCS beds: cross-laminated, very fine-grained basal sandstone (unit I) with intensely bioturbated middle portion (unit II) is overlain by a non-bioturbated clay-rich mudstone (unit III). If preserved, the upper bed portion appears to be modified via cryptobioturbation (CB, white arrows) the basal portion of sandstone S3 (tidal dunes), with well-developed current ripple lamination (black, continuous line) with tidal reactivation surfaces (black, thick continuous lines; BR). (c) Backscattered SEM micrograph of the fine-grained fraction in facies M3 showing silt-sized mica (Biotite, 'Bio') and quartz grains (Qz), embedded within a silt- and clay-sized illite-rich matrix (black arrows).

4.h. Facies M3: normally-graded mudstone

4.h.1. Description

Facies M3 makes up *c.* 25 % of the logged section at Ochre Cove (Fig. 8). M3 mudstones are developed as centimetre-thick, wavy-discontinuous very fine-grained siltstone and silty mudstone separated by one or, sometimes, two grain-size breaks (Figs 6a,b). The bases of single beds are subdivided into three parts. Fine-grained basal units (unit I) contain planar and cross-laminated siltstone with some pinch-and-swell lamination that occasionally also includes some very fine-grained sandstone (Fig. 6b). This latter unit is overlain by wavy laminated silty mudstone (unit II) and non- to sparsely bioturbated clay-rich mudstone (unit III) (Fig. 6b). The M3 bioturbation index is 0–1 (0–5 %). Bed tops contain rare compacted, sandstone-filled *Planolites*, very rare *Rosselia* and some biodeformation (Fig. 6a). Discrete lamina sets and bed boundaries appear disrupted and 'diffuse' (Fig. 6b). The framework of the mudstone-dominated unit III (Fig. 6c) facies is composed of subangular to rounded, fine- to medium-grained quartz, silt-sized lithic clasts, biotite, some plagioclase and muscovite. The matrix is composed predominantly of illite (Fig. 6c).

4.h.2. Interpretation

Preferential preservation of single centimetre-sized gutters filled with coarser-grained sandstone, in conjunction with well-developed grain-size breaks within mudstone (Fig. 6b), possibly indicates erosion of sand and bypass following gravity flow deposition. Preferential preservation of sandstone in open *Planolites* burrows highlights that initial coarser-grained bed tops (which infilled open *Planolites* burrows) might have been eroded (Fig. 6a). Diffuse laminae potentially indicate the presence of cryptobioturbation, attesting to the possibility of oxygenated pore waters following deposition (Gingras *et al.* 2011). Two prominent grain-size breaks between the basal very fine-grained sandstone (unit I), faintly laminated coarse siltstone (unit II) and the overlying sparsely to non-bioturbated mudstone (unit III) potentially support flow transformation during bed deposition, respectively during the waning phase of the sediment flow (Duke *et al.* 1991).

4.i. Facies M4: homogeneous mudstone

4.i.1. Description

The M4 mudstones comprise *c.* 10 % of the entire succession and are developed as centimetre- to decimetre-thick, highly continuous beds over several tens of metres, bound by erosive, wavy-continuous contacts (Fig. 7a). These mudstones are composed of silt-bearing, clay-rich mudstone that terminates with decimetre-thick, metre-wide carbonate lenses and decimetre-wide septarian concretions (Fig. 7a, b). Internally, M4 mudstones appear homogeneous and contain little evidence of bioturbation (BI 0–1; 0–5 %). Only very rarely isolated patches

https://doi.org/10.1017/S0016756819000402

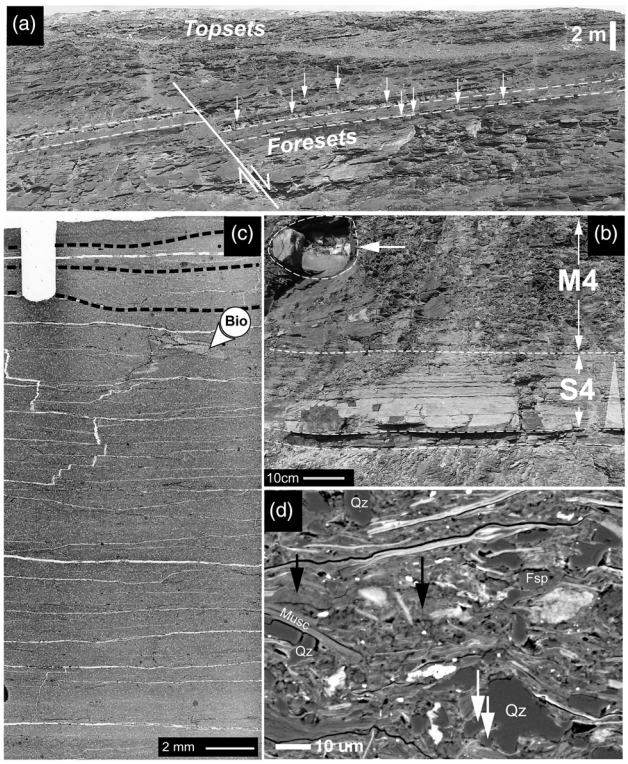

Fig. 7. Facies S4 and M4. (a) Outcrop panel showing the OCC topset and foreset. White arrows indicate positions of large septarian concretions, which seem to occur preferentially along bed contacts. A normal fault (white, continuous line) dissects the OCC. (b) Close-up of facies S4; graded bedding of medium- to coarse-grained sandstone S4. Note that large septarian concretions and lenses are concentrated at bed tops (white arrow). (c) Flat bed scan of M4 mudstone, which is faintly laminated (white, dashed lines), with 'floating' silt grains throughout the clay-rich matrix that also contain rare biodeformation structures (Bio). (d) Backscattered SEM micrograph of the fine-grained fraction in facies M4 showing silt-sized mica (Biotite, 'Bio'), feldspar (Fsp) and quartz grains (Qz) with overgrowths (white arrows), embedded in a pore-occluding illite-rich matrix (black arrows) and white mica (Musc).

of biodeformational and escape structures are visible in bed tops (Fig. 7c). The framework components include subangular to round, fine to medium silt-sized quartz, lithic clasts, biotite, some plagioclase and muscovite. The mudstone M4 matrix is composed predominantly of illite (Fig. 7c, d). The septarian concretions are composed of potentially ferroan carbonate.

4.i.2. Interpretation

The continuous nature of the M4 mudstone, in combination with a non-graded texture and the fact that it lies conformably above S4 sandstone, indicates that M4 mudstones could have been deposited by rapidly decelerating flows. These deposits are commonly observed on the clinothem foreset, and might indicate the final stage of deposition from potentially dilute density currents (Talling *et al.* 2012; Zavala & Arcuri, 2016). Longer periods of slower sediment accumulation produce excellent conditions for the growth of carbonate cement and the formation of ferroan carbonate lenses and septarian concretions (Föllmi, 2016) (Fig. 7b). Their stratigraphic relationship suggests that M4 mudstones are genetically related to underlying S4 sandstones. If those S4 sandstones originated from offshore-directed sediment gravity flows then the decimetre-thick, non-graded, upper M4 portion could originate from lofting and coeval suspension settling (Zavala & Pan, 2018).

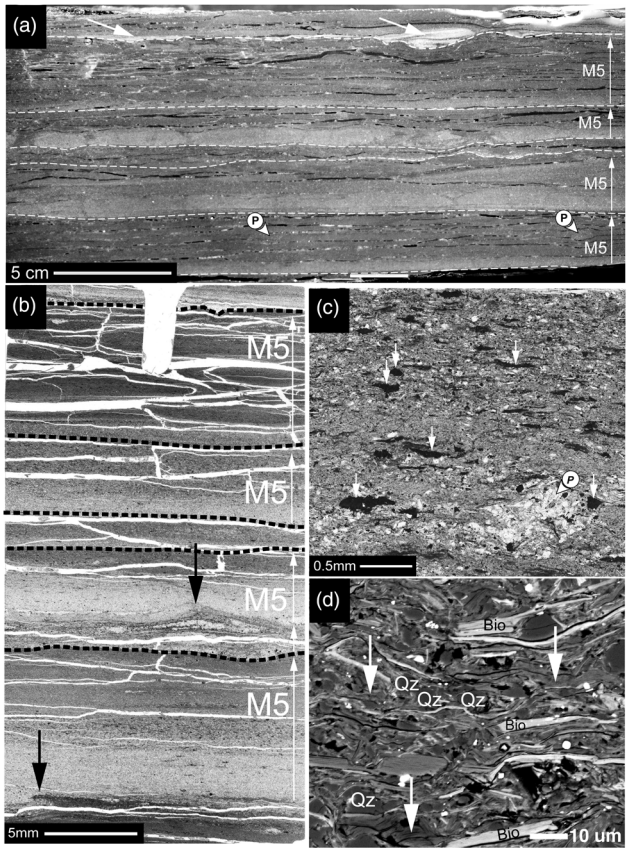

Fig. 8. Facies M5 (thin-bedded mudstone). (a) Polished hand sample showing centimetre-thick, wavy-continuous, normally-graded beds, many of which contain erosive tops (white dashed lines) and are sparsely bioturbated by shallow-tier *Trichophycus* (T). Centimetre-wide sandstone-filled gutters are occasionally preserved (white arrows). (b) Stacked, partially eroded beds contain coarse siltstone in the base, overlain by fine silt- and clay-rich mudstone. Soft-sediment deformation below these event beds (black arrows) is common. Sandstone-filled gutters are common at bed tops (white arrows). (c) Low-resolution micrograph showing the textural characteristics of a single, normally graded M5 bed. Wavy stringers of kerogen and possibly pyrite (white arrows) are dispersed throughout the mudstone (plane-polarized light). (d) Backscattered SEM micrograph of the fine-grained fraction in facies M5 showing silt-sized platy mica (biotite, 'Bio'), some silt-sized quartz (Qz), embedded within a pore-occluding illite-rich matrix (white arrows).

4.j. Facies M5: thin-bedded mudstone

4.j.1. Description

Thin-bedded mudstone comprises *c.* 20 % of the OCC (Fig. 2). M5 mudstone contains centimetre-thick, even and wavy-continuous beds with small, centimetre-sized sandstone-filled gutters (Fig. 8a, b). The M5 mudstone beds are normally graded with both even and cross-laminated coarse siltstone in the base and clay-rich mudstone. Beds are laterally continuous at the decimetre scale (Fig. 8a). Within millimetre-thick beds, siltier laminae form upward deformed flame structures (Fig. 8b). This facies is non-bioturbated to sparsely bioturbated (BI 0–1; 0–5 %) and contains millimetre-sized, sand-filled *Planolites*, *Trichophycus* and ample biodeformational structures preferentially concentrated close to bed tops. The framework components contain subangular to rounded, fine to medium silt-sized quartz, lithic clasts, biotite, and some plagioclase and muscovite (Fig. 8c). The mudstone matrix is composed predominantly of illite and some dark, wavy stringers of kerogen (Fig. 8c, d).

https://doi.org/10.1017/S0016756819000402

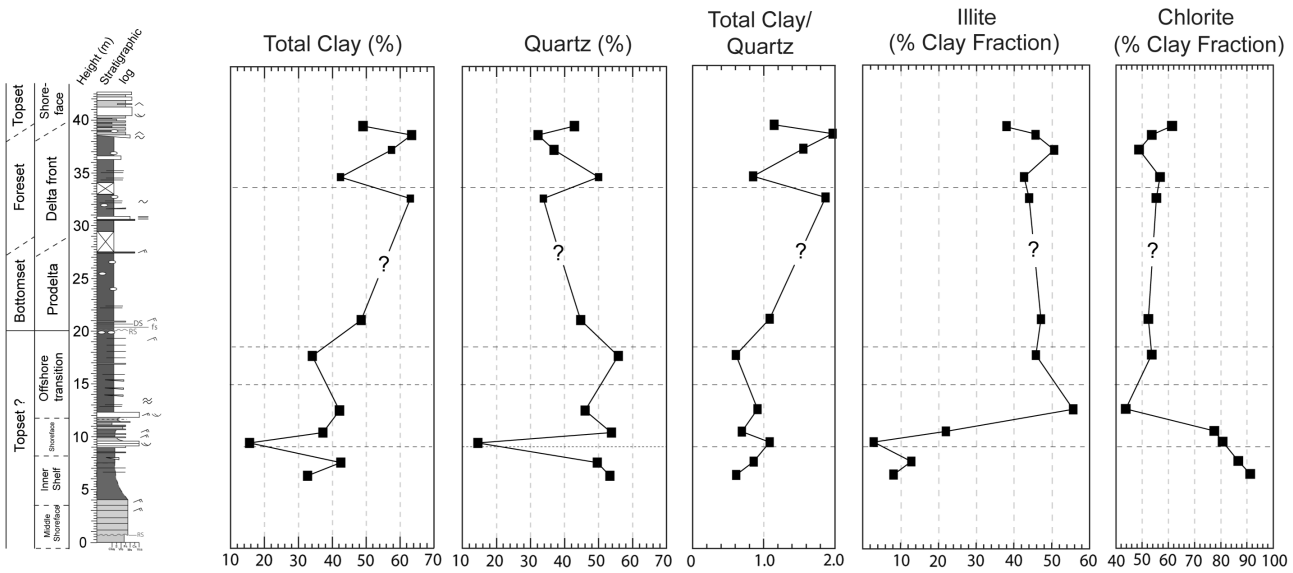

Fig. 9. The bulk and clay mineralogical composition of the studied interval at Ochre Cove. Note the overall increase in the ratio of clay minerals to quartz and the shift in the dominant clay mineral from chlorite to illite, which were recorded across ~10 m stratigraphic height.

4.j.2. Interpretation

Thin-bedded, laterally continuous mudstone beds with normal grading and occasional flame structures point towards relatively rapid deposition over an unconsolidated, preferentially mud-rich seabed (Fig. 8b). The clay-rich, non-bioturbated tops could originate from rapid deposition and burial. Thinner and finer-grained M2 beds were deposited below the fair-weather wave base, where only strong storms or density flows were able to rework the seafloor. Gutters filled with fine-grained sandstone with wavy-discontinuous lamination indicate occasional bed erosion via storms and bypass of coarser-grained sediment (Fig. 8a). The presence of flame structures indicates lateral drag in mud that was not yet fully dewatered when the following event bed has been deposited (e.g. Mills, 1983) (Fig. 8b). The dark stringers composed of both, pyrite and wavy opaque material might constitute allochthonous (or reworked?) kerogen (Harazim & McIlroy, 2015) (Fig. 8c, d).

4.k. Facies associations

4.k.1. FA1: wave- and current-reworked topsets

Sandstone facies S1 and S2, and mudstone facies M1–M3 share basal flat lamination and were therefore grouped into one facies association. In this, wave-ripple cross-lamination, trough cross-bedding and undulating lower bounding surfaces are indicative of bedform migration and potentially widespread seafloor erosion and bed removal (Figs 4–6). Elongate sandstone-filled scour structures (i.e. gutter casts) with ripple cross-lamination that are dipping transverse to scour axes are prominent for facies S3. Likewise, the disconnected, asymmetric, starved sandstone ripples (Fig. 5) equivalent to the same S3 facies could represent a part of the topset that is not directly influenced by frequent riverine sand supply (Catuneanu & Zecchin, 2013). Well-developed, unidirectional wave-reworked sandstone (S1), medium-grained, wave- and current-rippled sandstone (S2) interbedded with M1 and M2 all exhibit a high lateral continuity, similar (decimetre) thickness and were observed in facies that most likely belong to the clinoform topset (Fig. 2, Fig. 11 further below). Mud-rich facies M1, M2 and M3, located below 13 m stratigraphic height (Fig. 2), were grouped into this FA1 facies association due to their significantly higher amount of Fe-rich chlorite, compared to FA2 (Fig. 9).

4.k.2. Facies association 2 (FA2): gravity-flow dominated foresets and bottomsets

Planar-laminated sandstone (S4), homogeneous mudstone (M4) and thin-bedded mudstone (M5) exhibit high lateral continuity at the bedset scale and were almost exclusively observed on the clinothem bottom- and foreset, at above 20 m stratigraphic height (Fig. 2). Above 20 m, those latter mudstones also experience a substantial increase in illite/chlorite ratio. FA2 sandstone and mudstone facies exhibit very high aspect ratios, with graded bedding and well-developed grain-size breaks that terminate, in the case of facies M4, with stratiform septarian concretions and lenses (Figs 8–10).

5. Stratigraphic distribution of component minerals in the mud-dominated facies

About seven dominant minerals were identified by employing SEM petrography and whole-rock and clay-specific QXRD, of which only four were abundant enough (>5 wt %) to be relevant for discussion in clinothem building and progradation (Fig. 9).

Stratigraphic comparison of QXRD analyses (Fig. 9) shows significant mineralogical variability throughout the studied succession. The volume of clay minerals as a percentage of the total rock volume increases vertically through the succession. Non-clay silicate minerals (i.e. quartz and plagioclase), as a percentage of total rock volume, however, show variations decreasing from >50 % by volume at the base of the section to ~30–40 % at the top. A notable deviation from this trend is observed at ~9 m (Fig. 9), where non-clay silicates contribute to only ~14 % of the rock volume. Overall the ratio of clay minerals to non-clay silicates in the succession increases vertically. The composition of the clay minerals also varies within the succession. Chlorite, as a percentage of the clay mineral volume, sharply decreases throughout the succession from >90 % of the clay mineral assemblage at the base of the studied

https://doi.org/10.1017/S0016756819000402

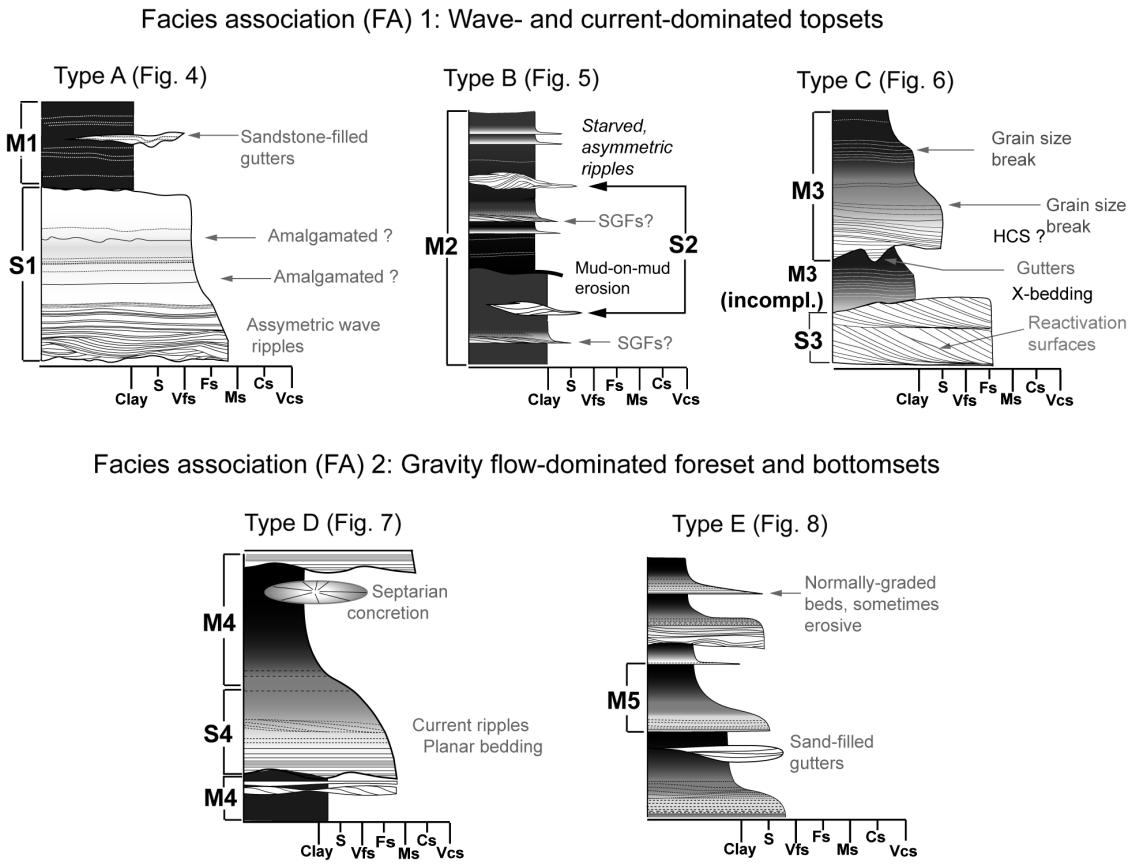

Fig. 10. The five characteristic, recurring bedset types A–E across the OCC depositional profile. Each bedset type contains at least one out of four sandstone (S1–4) and five mudstone (M1–5) facies. Bedset types and facies are summarized into two facies associations (FAs): FA1 (wave- and current-dominated topset) and FA2 (gravity-flow dominated foreset and bottomset).

succession to a low of 43 % at 12.5 m stratigraphic height (Fig. 9), above which the percentage of chlorite remains relatively constant at ~55 % of the clay mineral volume. Illite as a percentage of the clay mineral volume increases throughout the succession from <10 % at the base of the studied section to a maximum of 57 % at 12.5 m stratigraphic height, above which the percentage of illite remains relatively constant at ~45 %. Pyrite is observed as an accessory component, comprising <5 % of the total rock volume except for the lower 10 m of the exposure, where its higher volume coincides with the presence of pyritic sandstones described by Ranger *et al.* (1984).

6. Discussion

6.a. Process-based interpretation of event bed deposits

Bedset types are useful descriptors of mud depositional processes, because they preserve the mudstone depositional product as it evolves throughout successive stages of bed formation (erosion → settling → deposition → reworking), which then can result in the preservation of more than one stacked facies (Fig. 10). The fabric and texture of individual sandstone and mudstone beds depend on the initial sediment concentration and especially volume fraction of cohesive clay (Sumner *et al.* 2009). A change in flow viscosity and yield strength across orders of magnitude can be induced by adding even small amounts of clay to the suspension (e.g. Coussot, 2017), which, overall, controls if bedforms develop (Schieber & Southard, 2009). Five recurring mudstone bedset types (A–E) record sand and mud transport and depositional processes across the OCC depositional profile. Those bedset types are defined based upon mudstone grading, fabric and characteristics of subordinate sandstone beds and lenses, and are internally composed of at least two but often more than two lithofacies. This process-based interpretation of OCC mudstones is based upon an assemblage of well-described ancient sand- and mudstone deposits (Duke *et al.* 1991; Myrow & Southard, 1996; Clifton, 2007; Haughton *et al.* 2009; Macquaker *et al.* 2010; Talling *et al.* 2012; Plint, 2014; Poyatos-Moré *et al.* 2016; Birgenheier *et al.* 2017), experimental studies (Baas *et al.* 2011, 2013, 2016) and examples from the modern seafloor (Bentley & Nittrouer, 2003; Rotondo & Bentley, 2003; Denommee *et al.* 2016).

6.b. Deposition and reworking of mud in the OCC

Variability in lithofacies across the OCC is driven by (a) prominent change in bedding aspect ratio, (b) winnowing of grain size in more distal portions of the clinothem and (c) a gradual change from wave- to gravity-controlled deposition control (Fig. 11). This depositional setting produces bedsets composed of often multiple, stacked event beds with a wide range of grain sizes, which do not always show traditional (offshore-fining) facies distributions with increasing shoreline proximity. Normally-graded beds with erosive tops and palimpsest ichnofabric are formed on modern storm-dominated shelves, where large volumes of coarse-grained sediment are seasonally discharged via flashfloods and reworked across high-energy shelves (e.g. Eel Shelf; Milliman & Syvitski 1992; Ogston *et al.* 2000).

https://doi.org/10.1017/S0016756819000402

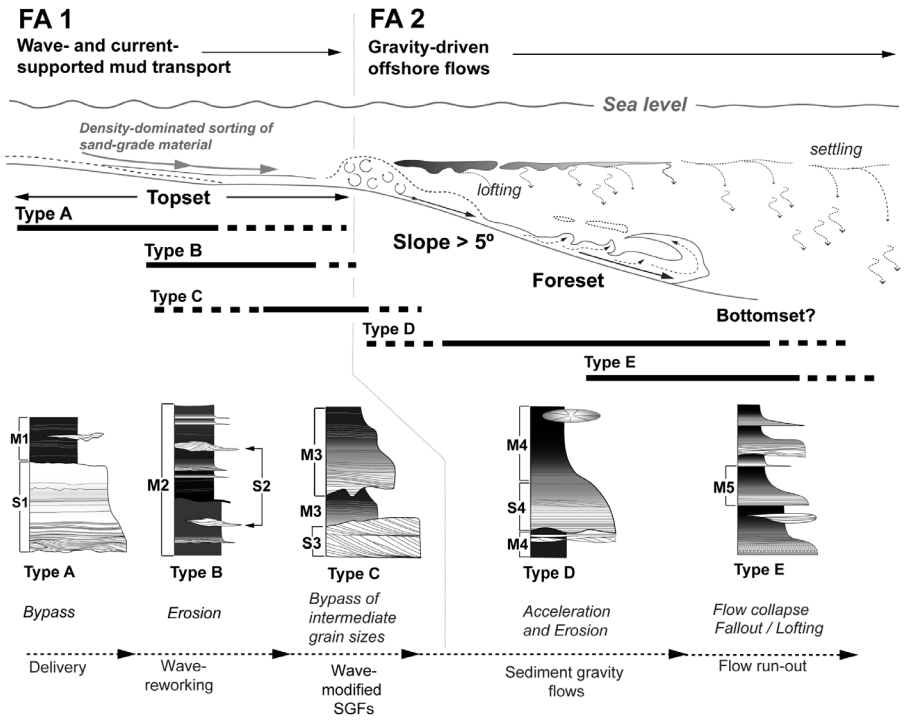

Fig. 11. Schematic block diagram showing the facies diversity, along with the distribution of bedset types across the OCC depositional profile.

FA1 deposits are inferred to originate from episodic, storm-driven event sedimentation. Storm conditions likely existed only for short, discrete periods within the clinothem topset depositional environments. Their influence on sediment transport and deposition, however, is disproportionately large because they are erosional and deposit thick beds (Clifton, 2007). When storms coincide with high fluvial discharge then large quantities of fine-grained sediment are discharged onto the shelf via deltas (Hill *et al.* 2001; Mulder *et al.* 2003). Storm-related discharge delivers a large amount of sand during heightened seasonal discharge (Zavala & Arcuri, 2016). This discharged, water-laden mixture of sand, water and mud forms bottom-hugging sediment laden suspensions that alternate between deposition and erosion, and can therby deposit complex composite beds (Zavala & Arcuri, 2016; Zavala & Pan, 2018).

Another possibility for the deposition of FA1 units is a potential slope failure. The resulting avalanching generates fully turbulent gravity flows (i.e. turbidity currents) with potentially long flow run-out distances (e.g. Haughton *et al.* 2009). Both sandstones and mudstones of FA1 were deposited by both unidirectional currents (Fig. 5) and waves (Fig. 7). In the sandstone fraction, centimetre- to decimetre-thick *Type A* bedsets preserve decimetre-length wavelength wave ripples, intra-bed erosional surfaces and very sharp grain-size changes (Fig. 10A). M1 mudstones contain internally little fabric evidence for bedload transport (i.e. neither widespread lamination, nor starved sandstone ripples or wavy-discontinuous lamination). Instead, M1 mudstones seem to record alternating pulsed sediment delivery events of sand and mud as well as frequent storm-dominated erosion and sediment bypass. The presence of sandstone-filled scours (Fig. 4b) represents a coarse-grained relict facies that could potentially indicate sediment bypass.

Starved fine- to medium-grained sandstone lenses (Fig. 5, *Type B* bedsets) with internally asymmetric wave ripples of S2 possibly originated during unidirectional transport and subsequent wave reworking (Duke *et al.* 1991). Millimetre-thick beds with a prominent triplet motif are common throughout this facies (Fig. 5c). M2 beds broadly resemble bed stratigraphy deposited by a number of density-driven mud-rich gravity flow types similar to current-wave-enhanced sediment gravity flows (CWESGFs) (Macquaker *et al.* 2010; Denommee *et al.* 2016), hyperpycnal flows (e.g. Mulder *et al.* 2003; Lamb & Mohrig, 2009) and turbidity currents (e.g. Haughton *et al.* 2009). Readily visible strataform, silty linings connecting starved sandstone ripples (Fig. 5b) were previously described as the product of migrating ripples that indicate forcing via unidirectional currents that prevailed at least during the waning phase of the flow (Schieber, 2016).

Repeated observance of intra-bed sedimentary fabrics within layers that contain this *Type B* bedset type that exhibit a triplet motif (unit a – turbulent traction transport and erosion; unit b – planar parallel laminae deposited during the laminar phase of flow; unit c – suspension settling as the flow wanes) (Fig. 5b) probably indicates a form of waning density flow that potentially experienced wave-influenced transport. However, true CWESGFs (*sensu* Friedrichs & Wright, 2004) require sufficient supply of detritally sourced fluidized muds to facilitate across-shelf mud transport (Wright *et al.* 2001; Bentley & Nittrouer, 2003). This condition is unlikely to have been met in the Power Steps Formation, since the original illite-dominated detrital clay–mineral fraction sourced from the Palaeozoic hinterland is relatively small (Harazim & McIlroy, 2015). Nevertheless, they might constitute some form of (wave-modified?) sediment gravity flow (SGF) (Fig. 5c).

Sandstones of *Type C* bedsets contain laterally continuous, cross-bedded sandstone with internal duplet structures and ample reactivation surfaces (Fig. 6a). Based on their unidirectional ripples and abundant reactivation surfaces, these sandstones are being interpreted as the product of tidal dune deposition that were deposited and preserved between storm events. Here as well,

https://doi.org/10.1017/S0016756819000402

well-developed grain-size breaks in overlying M3 facies indicate bypass of intermediate grain sizes, possibly as a result of increasing relative clay content during the waning phase of the storm (e.g. Coussot, 2017).

Sandstone-dominated tidal bedforms in facies S3 (Fig. 6a) and normally graded M3 mudstone are interpreted as the more distal equivalent of S1 sandstones and M1 mudstones. While storm-driven mud dispersal is inferred to have been episodic on the OCC, the presence of centimetre-thick, three-dimensional tidal bedforms indicates that the prevailing fair-weather sedimentation has been dominated by unidirectional tidally controlled sand transport. The absence of a fully developed hummocky cross-stratification in the base layer of M3 facies (Duke *et al.* 1991) might result from the fact that original grain-size distribution also contained higher amounts of cohesive clay.

Either way, the occurrence of *Type B* bedsets indicates that at one point muds were being advected alongshore, outside the reach of immediate sand supply where the shore-oblique geostrophic currents component increases in strength (Duke *et al.* 1991; Plint, 2014). The presence of short, asymmetric very fine-grained sandstone ripples and frequent large-scale (mud-on-mud) erosion events (Fig. 5b) perhaps indicates that more distal *Type C* bedsets experienced a higher preservation potential and more complete preservation of event stratigraphy compared to *Type A* or *B* bedsets, even though bed reworking frequency and intensity is proposed to have been broadly similar (see Fig. 11).

It is inferred that the storm-weather wave base (which is usually one order of magnitude deeper than the regional fair-weather wave base; Snedden *et al.* 1988) has changed across the OCC. The preservation potential of shelf currents seems to increase from the proximal to the distal portion of the clinothem topset where the majority of mud and sand is being moved offshore via unidirectional, river-flood hyperpycnal discharge. This offshore transport has, additionally, been modified by a combination of combined flows (consisting of wave-motion and long-shore directed geostrophic flows; Perillo *et al.* 2014) and, to some degree, by a density-driven offshore flow (Duke *et al.* 1991; Myrow & Southard, 1996).

At modern-day sea-level highstand (Skilbeck *et al.* 2017) some shelf areas often remain too gentle to initiate autosuspensive, gravity-dominated transport (i.e. as a turbidity current). The initiation of hyperpycnal turbidity currents requires a gradient of at least 0.7°, a flooding event, and high suspended sediment concentration (e.g. Wright *et al.* 2001; Mulder *et al.* 2003), conditions which are easily met in the studied section. With a measured slope of ~5° on the clinothem foreset (Fig. 6a), autosuspensive transport might easily have been initiated after pulsed flashfloods or earthquakes. The deposition of large volumes of initially non-weathered, sand-size grains and clasts, with a typical volcanic grain density of above 2.7 g cm^{-3}, could easily have produced clinoform foreset slopes in excess of 0.7°.

The OCC foreset and bottomset (FA2) are interpreted to represent exclusively pulsed sediment delivery and much longer breaks in sedimentation compared to FA1. This is based on the presence of laterally continuous, normally-graded event bed deposits with extensively cemented and concretionary bypass surfaces (Fig. 7a, b). Even-bedded and ripple cross-laminated S4 sandstone of *Type D* bedsets are encountered close to the clinothem rollover, most likely originated as dilute, fully turbulent density flows with relatively low sediment fall-out rate (Fig. 7b) that either formed in an area of flow expansion (close to an increase in clinothem slope; Kane & Hodgson, 2012; Poyatos-Moré *et al.* 2016) or as a result of river-fed hyperpycnal currents (Sumner *et al.* 2009). The prevalence of normal grading and absence of the preserved inversely graded lower bed portion within *Type D* bedsets indicate that those flows were potentially not always sustained (Bhattacharya & MacEachern, 2009). The overall absence of interlaminated sand–mud current ripples throughout FA2 suggests that flow deceleration times were probably short.

Palimpsest bioturbation in facies M4 indicates either erosion of the bioturbated bed tops, or indicates rapid sediment accumulation on the clinothem with insufficient time available for bed colonization by benthic organisms. The OCC bottom-set *Type E* bedsets, which are interpreted to represent the thinner, distal deposits of turbidite flow run-outs, include unidirectional current-ripples, composed of fine-silt to fine-sand grains. These can be observed to downlap onto basal scour surfaces, whereby internal lamina sets display continuous, planar, fining-upward grading (Fig. 8a, b). Those beds have been preferentially recorded above the OCC downlap surface 'DS' (Figs 2, 3) that also includes the most distal clinothem bottomset deposits.

6.c. The origin of mud in the Power Steps Formation

Combined SEM and transmission light microscopy as well as QXRD analyses reveal a highly variable illite and chlorite volume across the OCC. The silt- and clay-sized mineral assemblage of the M1 and M2 facies is primarily composed of iron-rich minerals, which are in large part of diagenetic origin. The presence of widespread replacement fabric and large volume of chloritized grains and lithoclasts (Figs 4, 5), combined with the unusually high hand sample weight, due to high matrix Fe content, indicates that the clay- and silt-sized sediment fraction has originated, at least partially through the riverine influx of higher volumes of non-stable, Fe-rich mafic and mechanically weathered components that were most likely sourced from an early Palaeozoic, non-vegetated hinterland (Tosca *et al.* 2010). Upon deposition, sand- and silt-sized mafic grains and lithoclast are chloritized within the sediment upon burial and temperature increase (e.g. Hower *et al.* 1976; Harazim & McIlroy, 2015). This *in situ* transformation of less stable minerals appears to be a common process in the Bell Island Group, as has already been demonstrated in muddy shoreface deposits of the stratigraphically lower-positioned Beach Formation (Harazim & McIlroy, 2015). An initially silt-sized pseudomatrix, composed of weathering-susceptible olivine and pyroxenes, now altered to Fe-rich chlorite (chamositic) cement engulfs subangular silt-sized quartz, biotite, and muscovite and plagioclase (Figs 4d, 5d).

Burial-diagenetic dissolution of volcanic ash can lead to the precipitation of a wide range of authigenic minerals, controlled by their starting composition as well as weathering susceptibility (Kiipli *et al.* 2007). The large amount of illite recorded in the upper part of the OCC might have originated from the subsequent smectite-to-illite transition and subsequent quartz cement precipitation. Higher silica activities in initially open pore space of the silt-rich fraction could explain the high modern-day abundance of quartz overgrowths (Fig. 7d) and extensive pore-occluding illite (Figs 6–8) (e.g. van de Kamp, 2008).

6.d. Clinothem architecture

Deltaic slopes in excess of ~0.7° are not very common for modern-day transgressive shorelines (Boyd, 2010; Denommee *et al.* 2016). With a much steeper foreset the OCC does therefore provide a unique window into how mud has been deposited and

https://doi.org/10.1017/S0016756819000402

converted into mudstone across an early Palaeozoic delta. Previous sedimentologic investigations of the underlying Tremadocian Beach (Harazim & McIlroy, 2015) and Redmans formations (Miller & McIlroy, 2014) revealed that autocyclic changes in the supply of silt- and sand-sized detrital components dominate the stratigraphic and compositional variability of each respective depositional setting. On the OCC, outcrop-wide exposure of event beds allows correlation between all described bedset types and facies across the depositional profile, leading to the proposal of a sedimentological depositional dip-parallel model (Fig. 11). This model highlights that with increasing distance from the riverine dispersal system the relative thicknesses of storm-dominated mudstones (*Type A* and *B* bedsets) tend to become thinner, while bed continuity increases in the offshore direction (*Type C* bedsets). The *Type D* to *E* bedsets of more distal FA2 deposits highlight that much of the sediment transport to foreset and bottomset positions has been facilitated via sediment gravity flows. Well-cemented event bed tops attest that longer periods of non-deposition and bypass accompanied offshore-directed sand and mud transport across the OCC, via sustained delivery of river-fed sediment and potential slope failure at the comparatively steep delta front (Fig. 3) (Clare *et al.* 2016). The continuous facies succession of a prograding clinothem from distal offshore muds to thick, amalgamated topset sandstone is inferred for the clinothem portion above 20 m stratigraphic height. The underlying shoreface–shelf succession below 20 m stratigraphic height, however, does not show a classic onshore–offshore facies succession (*sensu* Aigner & Reineck, 1982; Clifton, 2007; Plint, 2010). Instead, it is interpreted to represent a small number of amalgamated and incomplete parasequences, most likely linked to episodic, partial bed removal and sediment bypass on the OCC delta top. In order to explain the observed contrast in mudstone composition across the OCC not only the delivery mechanism is considered, but also the density contrasts among the original mineralogical assemblage, which is inferred to have included highly variable amounts of volcanoclastic material. The inferred hydrodynamic 'sieving' of sand-sized mafic higher-density grains (i.e. olivine, pyroxene, amphibole) and mafic lithoclasts (versus quartz) (Fig. 4d) closer to the shoreline might explain the prominent shift in the chlorite/illite ratio at ~10 m stratigraphic height (Fig. 9). The increase in overall clay content (Fig. 9) as well as the increase in the ratio of mudstone to sandstone beds is interpreted to coincide with increasing shoreline proximity and water depth.

It is proposed that the wave-induced turbulence remained insufficient on the OCC to maintain this high iron, high density mineral assemblage of riverine-sourced, sand-sized mafic mineral and lithoclasts in suspension as the water deepened and/or wave-orbital velocities waned. However, combined, wave–current flows that involve two forcing mechanisms, and are therefore more effective at sediment transport than waves or currents alone (e.g. Grant & Madsen, 1986), could have facilitated offshore-directed sediment transport.

The observed onshore–offshore change in grain size and clay origin (Figs 9, 11) most likely reflects a change in input volume and frequency of high volumes of unstable mafic detritus as well as feldspar (as a result of changing volcanic activity), or a more direct change in transport path, possibly via autocyclic river avulsion and shifting distributory channels (e.g. Catuneanu & Zecchin, 2013). The overall coarse grain-size distribution of the proto-mud fraction within OCC deposits and the general absence of widespread cohesive clay in the Bell Island Group (Harazim & McIlroy, 2015) might explain the steep nature of the OCC, as well as its relatively small size compared to other, larger clinothem systems that extend over several tens to hundreds of kilometres (Johannessen & Steel, 2005; Pattison *et al.* 2007; Varban & Plint, 2008; Patruno *et al.* 2015; Poyatos-Moré *et al.* 2016).

7. Conclusions

The OCC on Bell Island, Newfoundland, serves as a key archive for understanding the sedimentology and diagenesis of early Palaeozoic shelves, where most of its detrital components have been delivered via mechanical weathering from a non-vegetated hinterland. Based on our integrated sedimentological and compositional analyses, the facies architecture of the OCC can be genetically linked to: (1) deltaic sediment input; (2) offshore- and alongshore-directed sediment dispersal driven by storm waves and unidirectional currents; and (3) relative chemical grain stability during burial and diagenesis.

Detailed facies analyses reveal that sediment transport on the different architectural elements of the muddy shelf clinothem (i.e. the shoreface topset, foresets and inner shelf bottomsets) was driven by different mechanisms that reflect local hydrodynamic conditions. In proximal regions of the shelf clinothem, wave processes transported relatively coarse-grained sediment while in more seaward environments, currents play an increasingly important role in sediment transport, whereby the combined energies of waves and currents are capable of transporting relatively coarse-grained sediments when wave-orbital velocities alone are insufficient. Waves are inferred to influence sand and mud dispersal even across foreset and bottomset regions and therefore suggest much of the OCC has been deposited above storm-wave base.

A portion of the present-day clay mineral fraction represents the alteration product of highly unstable mafic (lithic) grains that were delivered to the shelf as silt-sized particles where they formed a fraction of the framework components. These lithic fragments were diagenetically altered to chlorite before significant compaction occurred. It is important to consider this fraction of the chlorite in the rocks separately from detrital chlorite when using clay mineralogy as a proxy for provenance.

The early Palaeozoic rocks on and around Bell Island capture a critical role in our developing understanding of how fine-grained, early Palaeozoic clastic dispersal systems functioned; especially since they provide a gateway to examine the conditions of *in situ* clay mineral production, prior to the evolution of widespread soil-based clay mineral factories from the Devonian onwards. To test the robustness and validity of *in situ* weathering, as an important 'clay factory' through pre-Devonian time, it will require more rigorous sedimentological analysis of more exposures on Bell Island and in the Conception Bay area as well as expansion of this research effort into similar successions which are even older.

Acknowledgements. This work was supported by the Billy and Anne Harrison endowment for sedimentary geology (S.J.B.) and by student research grants from the American Association of Petroleum Geologists (AAPG), the Geological Society of America (GSA) and the Society for Sedimentary Geology (SEPM) awarded to K.C.D. Rick Young (Louisiana State University) is thanked for his assistance with hand specimen preparation, and Wanda LeBlanc (Louisiana State University) is thanked for performing all QXRD analyses. Dr Sven O. Egenhoff is thanked for reviewing an early version of the manuscript.

https://doi.org/10.1017/S0016756819000402

References

Aigner T and Reineck H-E (1982) Proximality trends in modern storm sands from the Helgoland Bight (North Sea) and their implications for basin analysis. *Senckenbergiana Maritima* **14**, 183–215.

Austermann G (2016) *Sedimentology and depositional environment of the middle Cambrian Manuels River Formation in the type locality at Conception Bay South, Newfoundland, Canada*. Universität Heidelberg, Heidelberg, 356 pp. Unpublished thesis.

Baas JH, Best JL and Peakall J (2011) Depositional processes, bedform development and hybrid bed formation in rapidly decelerated cohesive (mud–sand) sediment flows. *Sedimentology* **58**, 1953–87.

Baas JH, Best JL and Peakall J (2016) Predicting bedforms and primary current stratification in cohesive mixtures of mud and sand. *Journal of the Geological Society* **173**, 12–45.

Baas JH, Davies AG and Malarkey J (2013) Bedform development in mixed sand–mud: the contrasting role of cohesive forces in flow and bed. *Geomorphology* **182**, 19–32.

Bentley SJ and Nittrouer CA (2003) Emplacement, modification, and preservation of event strata on a flood-dominated continental shelf: Eel Shelf, Northern California. *Continental Shelf Research* **23**, 1465–93.

Bentley SJ, Sheremet A and Jaeger JM (2006) Event sedimentation, bioturbation, and preserved sedimentary fabric: field and model comparisons in three contrastic marine settings. *Continental Shelf Research* **26**, 2108–24.

Bhattacharya JP and MacEachern JA (2009) Hyperpycnal rivers and prodeltaic shelves in the Cretaceous Seaway of North America. *Journal of Sedimentary Research* **79**, 184–209.

Birgenheier LP, Horton B, McCauley AD, Johnson CL and Kennedy A (2017) A depositional model for offshore deposits of the lower Blue Gate Member, Mancos Shale, Uinta Basin, Utah, USA. *Sedimentology* **64**. doi: 10.1111/sed.12359.

Bjørlykke K (1998) Clay mineral diagenesis in sedimentary basins – a key to the prediction of rock properties. Examples from the North Sea Basin. *Clay Minerals* **33**, 15–34.

Boyd R (2010) Transgressive wave-dominated coasts. *Facies Models* **4**, 265–94.

Brenchley PJ, Pickerill RK and Stromberg SG (1993) The role of wave reworking on the architecture of storm sandstone facies, Bell Island Group (Lower Ordovician), eastern Newfoundland. *Sedimentology*, **40**, 359–82.

Bruckner WD (1969) Geology of eastern part of Avalon peninsula, Newfoundland: a summary. In *North Atlantic: Geology and Continental Drift. International Conference, Gander, Newfoundland, 1967 Symposium*. Tulsa, Oklahoma: American Association of Petroleum Geologists, Memoir no. 12, pp. 130–8.

Buatois LA, Saccavino LL and Zavala C (2011) Ichnologic signatures of hyperpycnal flow deposits in Cretaceous river-dominated deltas, Austral Basin, southern Argentina. In *Sediment Transfer from Shelf to Deep Water – Revisiting the Delivery System* (eds RM Slatt and C Zavala), pp. 153–70. Tulsa, Oklahoma: American Association of Petroleum Geologists. AAPG Studies in Geology 61.

Campbell CV (1967) Lamina, lamina set, bed and bedset. *Sedimentology* **8**, 7–26.

Catuneanu O and Zecchin M (2013) High-resolution sequence stratigraphy of clastic shelves II: controls on sequence development. *Marine and Petroleum Geology* **39**, 26–38.

Cattaneo A, Correggiari A, Langone L and Trincardi F (2003) The late-Holocene Gargano subaqueous delta, Adriatic shelf: sediment pathways and supply fluctuations. *Marine Geology* **193**, 61–91.

Cattaneo A, Trincardi F, Asioli A and Correggiari A (2007) The Western Adriatic shelf clinoform: energy-limited bottomset. *Continental Shelf Research* **27**, 506–25.

Clare MA, Clarke JH, Talling PJ, Cartigny MJB and Pratomo DG (2016) Preconditioning and triggering of offshore slope failures and turbidity currents revealed by most detailed monitoring yet at a fjord-head delta. *Earth and Planetary Science Letters* **450**, 208–20.

Clifton HE (2007) A re-examination of facies models for clastic shorelines. In *Facies Models Revisited* (eds HW Posamentier and RG Walker), pp. 293–339. Tulsa, Oklahoma: SEPM, Special Publication 84.

Cocks LRM and Torsvik TH (2002) Earth geography from 500 to 400 million years ago: a faunal and palaeomagnetic review. *Journal of the Geological Society* **159**, 631–44.

Coussot P (2017) *Mudflow Rheology and Dynamics*. London: Routledge, 232 pp.

Denommee KC, Bentley SJ, Harazim D and Macquaker JHS (2016) Hydrodynamic controls on muddy sedimentary fabric development: Atchafalaya Chenier Plain subaqueous delta. *Marine Geology* **382**, 162–75.

Duke WL, Arnott R and Cheel RJ (1991) Shelf sandstones and hummocky cross-stratification: new insights on a stormy debate. *Geology* **19**, 625–8.

Egenhoff SO and Fishman NS (2013) Traces in the dark: –sedimentary processes and facies gradients in the upper shale member of the Upper Devonian–Lower Mississippian Bakken Formation, Williston Basin, North Dakota, USA. *Journal of Sedimentary Research* **83**, 803–24.

Eidam EF, Nittrouer CA, Ogston AS, DeMaster DJ, Liu JP, Nguyen TT and Nguyen TN (2017) Dynamic controls on shallow clinoform geometry: Mekong Delta, Vietnam. *Continental Shelf Research* **147**, 165–81.

Föllmi KB (2016) Sedimentary condensation. *Earth-Science Reviews* **152**, 143–80.

Friedrichs CT and Wright LD (2004) Gravity-driven sediment transport on the continental shelf implications for equilibrium profiles near river mouths. *Coastal Engineering* **51**, 795–811.

Gingras MK, MacEachern JA and Dashtgard SE (2011) Process ichnology and the elucidation of physico-chemical stress. *Sedimentary Geology* **237**, 115–34.

Grant WD and Madsen OS (1986) The continental-shelf bottom boundary layer. *Annual Review of Fluid Mechanics* **18**, 265–305.

Hanebuth TJ, Lantzsch H and Nizou J (2015) Mud depocenters on continental shelves – appearance, initiation times, and growth dynamics. *Geo-Marine Letters* **35**, 487–503.

Harazim D and McIlroy D (2015) Mud-rich density-driven flows along an early Ordovician storm-dominated shoreline: implications for shallow-marine facies models. *Journal of Sedimentary Research* **85**, 509–28.

Harazim D, McIlroy D, Edwards NP, Wogelius RA, Manning PL, Poduska KM, Layne GD, Sokaras D, Alonso-Mori R and Bergmann U (2015) Bioturbating animals control the mobility of redox-sensitive trace elements in organic-rich mudstone. *Geology* **43**, 1007–10.

Hart BS, Macquaker JH and Taylor KG (2013) Mudstone ('shale') depositional and diagenetic processes: implications for seismic analyses of source-rock reservoirs. *Interpretation* **1**, B7–B26.

Haughton P, Davis C, McCaffrey W and Barker S (2009) Hybrid sediment gravity flow deposits – classification, origin and significance. *Marine and Petroleum Geology* **26**, 1900–18.

Hill PS, Voulgaris G and Trowbridge JH (2001) Controls on floc size in a continental shelf bottom boundary layer. *Journal of Geophysical Research* **106**, 9543–9.

Hower J, Eslinger EV, Hower ME and Perry EA (1976) Mechanism of burial metamorphism of argillaceous sediment: 1. Mineralogical and chemical evidence. *Geological Society of America Bulletin* **87**, 725–37.

Jaramillo S, Sheremet A, Allison MA, Reed AH and Holland KT (2009) Wave-mud interactions over the muddy Atchafalaya subaqueous clinoform, Louisiana, United States: wave-supported sediment transport. *Journal of Geophysical Research: Oceans* **114**, C04002. doi: 10.1029/2008JC004821.

Johannessen EP and Steel RJ (2005) Shelf-margin clinoforms and prediction of deep-water sands. *Basin Research* **17**, 521–50.

Kane I and Hodgson DM (2015) Supercritical-flow structures on a Late Carboniferous delta front: Sedimentologic and paleoclimatic significance: Comment. *Geology* **43**, 374.

Kiipli T, Kiipli E, Kallaste T, Hints R, Somelar P and Kirsimäe K (2007) Altered volcanic ash as an indicator of marine environment, reflecting pH and sedimentation rate – example from the Ordovician Kinnekulle bed of Baltoscandia. *Clays and Clay Minerals* **55**, 177–88.

Lamb MP and Mohrig D (2009) Do hyperpycnal-flow deposits record river-flood dynamics? *Geology* **37**, 1067–70.

Laycock DP, Pedersen PK, Montgomery BC and Spencer RJ (2017) Identification, characterization, and statistical analysis of mudstone aggregate clasts, Cretaceous Carlile Formation, Central Alberta, Canada. *Marine and Petroleum Geology* **84**, 49–63.

Lazar OR, Bohacs KM, Macquaker JHS, Schieber J and Demko TM (2015) Integrated approach for the nomenclature and description of the spectrum of fine-grained sedimentary rocks. *Journal of Sedimentary Research* **85**, 230–46.

Li Z and Schieber J (2018) Composite particles in mudstones: examples from the late cretaceous Tununk shale member of the Mancos shale formation. *Journal of Sedimentary Research* **88**, 1319–44.

Macquaker JHS, Bentley SJ and Bohacs KM (2010) Wave-enhanced sediment-gravity flows and mud dispersal across continental shelves: reappraising sediment transport processes operating in ancient mudstone successions. *Geology* **38**, 947–50.

Miller HG (1983) A geophysical interpretation of the geology of Conception Bay, Newfoundland. *Canadian Journal of Earth Sciences* **20**, 1421–33.

Miller T and McIlroy D (2014) Sedimentology and stratigraphy of a wave-dominated delta from the Early Ordovician Redmans Formation, Bell Island, Newfoundland. In *ICHNOLOGY: Papers from ICHNIA III* (ed. D McIlroy), pp. 179–96. St John's, Newfoundland: Geological Association of Canada. Miscellaneous Publication 9.

Milligan TG, Ogston AS, Puig P, Scully ME, Traykowski PA and Wheatcroft RA (2007) Sediment delivery to the seabed on continental margins. In *Continental-Margin Sedimentation: From Sediment Transport to Sequence Stratigraphy* (eds CA Nittrouer, JA Austin, ME Field, JH Kravitz, JPM Syvitski and PL Wiberg), pp. 49–100. International Association of Sedimentologists, Special Publication no. 37. Malden, Massachusetts: Blackwell.

Milliman JD and Syvitski JP (1992) Geomorphic/tectonic control of sediment discharge to the ocean: the importance of small mountainous rivers. *The Journal of Geology*, **100**, 525–44.

Mills PC (1983) Genesis and diagnostic value of soft-sediment deformation structures – a review. *Sedimentary Geology* **35**, 83–104.

Moore DM and Reynolds RCJ (1997) *X-Ray Diffraction and the Identification and Analysis of Clay Minerals*. New York: Oxford University Press, 378 pp.

Mulder T, Syvitski JP, Migeon S, Faugeres J-C and Savoye B (2003) Marine hyperpycnal flows: initiation, behavior and related deposits: a review. *Marine and Petroleum Geology* **20**, 861–82.

Myrow PM and Southard JB (1996) Tempestite deposition. *Journal of Sedimentary Research* **66**, 875–87.

Ogston AS, Cacchione DA, Sternberg RW and Kineke GC (2000) Observations of storm and river flood-driven sediment transport on the northern California continental shelf. *Continental Shelf Research* **20**, 2141–62.

Patruno S, Hampson GJ and Jackson CAL (2015) Quantitative characterisation of deltaic and subaqueous clinoforms. *Earth-Science Reviews* **142**, 79–119.

Pattison SA, Ainsworth BR and Hoffman TA (2007) Evidence of across-shelf transport of fine-grained sediments: turbidite-filled shelf channels in the Campanian Aberdeen Member, Book Cliffs, Utah, USA. *Sedimentology* **54**, 1033–64.

Perillo MM, Best JL and Garcia MH (2014) A new phase diagram for combined-flow bedforms. *Journal of Sedimentary Research* **84**, 301–13.

Petschick R (2001) *MacDiff, freeware scientific graphical analysis software for X-ray diffraction profiles*. Frankfurt.

Plint AG (2010) Wave- and storm-dominated shoreline and shallow marine systems. In *Facies Models*, 4th edn (eds RW Dalrymple and NJ James), 167–99. St John's, Newfoundland: Geological Association of Canada.

Plint AG (2014) Mud dispersal across a Cretaceous prodelta: storm-generated, wave-enhanced sediment gravity flows inferred from mudstone microtexture and microfacies. *Sedimentology* **61**, 609–47.

Plint GA, Macquaker JHS and Varban B (2012) Bedload transport of mud across a wide, storm-influenced ramp: Cenomanian–Turonian Kaskapau Formation, Western Canada Foreland Basin. *Journal of Sedimentary Research* **82**, 801–22.

Poppe LJ, Paskevich VF, Hathaway JC and Blackwood DS (2001) A laboratory manual for X-ray powder diffraction. *US Geological Survey Open-File Report* **1**, 1–88.

Potter PE, Maynard JB and Depetris PJ (2005) *Mud and Mudstones, Introduction and Overview*. Berlin and Heidelberg: Springer, 297 pp.

Poyatos-Moré, M, Jones GD, Brunt RL, Hodgson DM, Wild RJ and Flint SS (2016) Mud-dominated basin-margin progradation: processes and implications. *Journal of Sedimentary Research* **86**, 863–78.

Ranger MJ, Pickerill RK and Fillion D (1984) Lithostratigraphy of the Cambrian - Lower-Ordovician - Bell Island and Wabana Groups of Bell, Little-Bell, and Kellys Islands, Conception Bay, Eastern Newfoundland. *Canadian Journal of Earth Sciences* **21**, 1245–61.

Rotondo KA and Bentley SJ (2003) Deposition and resuspension of fluid mud on the western Louisiana inner shelf, Gulf Coast Association of Geological Societies. *Transactions* **53**, 722–31.

Schieber J (1999) Distribution and deposition of mudstone facies in the Upper Devonian Sonyea Group of New York. *Journal of Sedimentary Research* **69**, 909–25.

Schieber J (2016) Mud re-distribution in epicontinental basins – exploring likely processes. *Marine and Petroleum Geology* **71**, 119–33.

Schieber J and Southard JB (2009) Bedload transport of mud by floccule ripples: direct observation of ripple migration processes and their implications. *Geology* **37**, 483–86.

Schieber J, Southard JB and Schimmelmann A (2010) Lenticular shale fabrics resulting from intermittent erosion of water-rich muds: interpreting the rock record in the light of recent flume experiments. *Journal of Sedimentary Research* **80**, 119–28.

Schieber J and Yawar Z (2009) A new twist on mud deposition: mud ripples in experiment and rock record. *The Sedimentary Record* **7**, 4–8.

Shanmugam G (2018) A global satellite survey of density plumes at river mouths and at other environments: plume configurations, external controls, and implications for deep-water sedimentation. *Petroleum Exploration and Development* **45**, 640–61.

Shchepetkina A, Gingras MK, Zonneveld JP and Pemberton SG (2017) Silt- and bioclastic-rich flocs and their relationship to sedimentary structures: modern observations from the petitcodiac river estuary. *Estuaries and Coasts* **40**, 947–66.

Skilbeck CG, Heap AD and Woodroffe CD (2017) Geology and sedimentary history of modern estuaries. In *Applications of Paleoenvironmental Techniques in Estuarine Studies*, pp. 45–74. Dordrecht: Springer.

Snedden JW, Nummedal D and Amos AF (1988) Storm- and fairweather combined flow on the central Texas continental shelf. *Journal of Sedimentary Research* **58**, 580–95.

Sumner EJ, Talling PJ and Amy LA (2009) Deposits of flows transitional between turbidity current and debris flow. *Geology* **37**, 991–4.

Talling PJ, Masson DG, Sumner EJ and Malgesini G (2012) Subaqueous sediment density flows: depositional processes and deposit types. *Sedimentology* **59**, 1937–2003.

Taylor AM and Goldring R (1993) Description and analysis of bioturbation and ichnofabric. *Journal of the Geological Society* **150**, 141–148.

Tosca NJ, Johnston DT, Mushegian A, Rothman DH, Summons RE and Knoll AH (2010) Clay mineralogy, organic carbon burial, and redox evolution in Proterozoic oceans. *Geochimica et Cosmochimica Acta* **74**, 1579–1592.

Van de Kamp PC (2008) Smectite-illite-muscovite transformations, quartz dissolution, and silica release in shales. *Clays and Clay Minerals* **56**, 66–81.

Van Staal CR, Barr SM and Murphy JB (2012) Provenance and tectonic evolution of Ganderia: constraints on the evolution of the Iapetus and Rheic oceans. *Geology* **40**, 987–90.

Varban BL and Plint GA (2008) Palaeoenvironments, palaeogeography, and physiography of a large, shallow, muddy ramp: late Cenomanian-Turonian Kaskapau Formation, Western Canada foreland basin. *Sedimentology* **55**, 201–33.

Williams H (1979) Appalachian orogen in Canada. *Canadian Journal of Earth Sciences* **16**, 792–807.

Wright LD, Friedrichs CT, Kim SC and Scully ME (2001) Effects of ambient currents and waves on gravity-driven sediment transport on continental shelves. *Marine Geology* **175**, 25–45.

Zavala C and Arcuri M (2016) Intrabasinal and extrabasinal turbidites: origin and distinctive characteristics. *Sedimentary Geology* **337**, 36–54.

Zavala C and Pan S (2018) Hyperpycnal flows and hyperpycnites: origin and distinctive characteristics. *Lithologic Reservoirs* **30**, 1–18.